A Two-Dimensional Relaxation Scheme for the Hybrid Modelling of Gas-Particle Two-Phase Flows

Kateryna Dorogan, Jean-Marc Hérard

A Two-Dimensional Relaxation Scheme for the Hybrid Modelling of Gas-Particle Two-Phase Flows

Kateryna Dorogan[1,2], Jean-Marc Hérard[1]
[1] Department of Fluid Dynamics, Power Generation and Environment,
EDF R&D, 6 quai Watier, 78400 Chatou, France
[2] LATP, CMI, 39 rue Joliot Curie, 13453 Marseille, France

March 29, 2012

Abstract

This paper presents a two-dimensional relaxation scheme for the hybrid modelling of two-phase gas-particle flows. The method is grounded on a previous relaxation scheme that has been proposed to cope with one-dimensional flows. One of the main difficulties here is due to the fact that the Reynolds tensor occuring in the Lagrangian framework is highly anisotropic. The interface relaxation scheme mimics a previously proposed "relaxation scheme" that involves GNL fields. The method is described and its main properties are given, including a short stability analysis, and numerical results are eventually provided.

Introduction

This paper deals with the modelling and the numerical simulation of polydispersed turbulent two-phase flows, where one phase is a turbulent fluid (considered to be a continuum) and the other appears as separate inclusions carried by the fluid (solid particles, droplets or bubbles). Such a kind of flows can be encountered in many industrial situations (combustion, water sprays, smokes) and in some environmental problems. Despite the need of their accurate prediction, the physical complexity of these processes is so broad that existing methods are either too expensive (in calculation cost) or not sufficiently accurate.

A hybrid approach was proposed in [10] in order to cope with one-dimensional flows, which consists in enlarging the size of the Eulerian set

of equations, in order to retrieve a natural upwinding of so-called source terms corresponding to the divergence of the Reynolds stress tensor. In a one dimensional framework, this approach may be confused with classical relaxation schemes used for the numerical approximation of solutions of barotropic Euler equations (see [3, 6, 8, 18, 25]). The main point is that in the 1D case, the -unique- Reynolds stress component may be viewed as a pressure field, whereas in the multi-dimensional case the -possibly high- anisotropy of the Reynolds stress tensor inhibits such an analogy. Therefore, one needs to introduce another -more complex- relaxation system for such a purpose.

As emphasized in [10], a first proposal was made which consists in mimicing the natural evolution equations of the Reynolds stress tensor, which may be easily derived (see [17], and also [16] which give some very first ideas in that direction). Such a procedure enables to recover a correct upwinding of complex multi-D waves that may pollute -and even blow out- numerical approximations obtained with more naive Riemann type solvers, for instance those relying of Euler type solvers (see for instance [21] and also [4] that exhibits a very simple instability pattern arising with Euler-type solvers). A drawback of this approach is that it requires enforcing *a priori* approximate jump conditions which can hardly be assessed. This motivates investigating true relaxation techniques involving only linearly degenerate fields, which is precisely what will be done within this paper.

The system of governing equations for the mean particle concentration α_p^E , the mean flow rate $\alpha_p^E \langle U_{p,i}^E \rangle$, which represents an Eulerian description of the particle phase, may be written as follows:

$$\partial_t \alpha_p^E + \partial_{x_i} \left(\alpha_p^E \left\langle U_{p,i}^E \right\rangle \right) = 0$$

$$\partial_t \left(\alpha_p^E \langle U_{p,i}^E \rangle \right) + \partial_{x_j} \left(\alpha_p^E \left(\langle U_{p,i}^E \rangle \langle U_{p,j}^E \rangle + \langle u_{p,i} u_{p,j} \rangle^L \right) \right) = \alpha_p^E g_i + \alpha_p^E \left\langle U_{r,i} / \tau_p \right\rangle^L \tag{1}$$

These are deduced from a Lagrangian formulation (see [7]), where the right-hand side terms represent the gravity and drag forces respectively. Obviously, the Reynolds stress term $\langle u_{p,i} u_{p,j} \rangle^L$ in system (1) must be provided by some external Lagrangian code, as occurs in the 1D case. We recall that the hybrid approach consists in solving simultaneously Eulerian system (1) and its Lagrangian counterpart, which in turn provides everywhere and at any time all components of the Reynolds stress tensor. Besides, the Eulerian model provides the values of $\langle U_{p,i}^E \rangle$ expected free from any statistical error, that should enable computations with a smaller number of particles in the Lagrangian code.

In the sequel, we omit the superscripts *"E"* and subscripts *"p"*, and intro-

duce the -constant- density of particles ρ_p. We denote by $\rho = \alpha_p^E \rho_p$ the mean density distribution of the particles in the domain, by $U_i = \left\langle U_{p,i}^E \right\rangle, i = 1,2$ the mean particle velocity. Hence, for given non-smooth values of the Lagrangian Reynolds stress tensor $\underline{\underline{R}}_{ij}^L = \langle u_{p,i} u_{p,j} \rangle^L$, we want to compute stable approximations of solutions of:

$$\begin{array}{l} \partial_t \rho + \partial_{x_j}(\rho U_j) = 0 \\ \partial_t(\rho U_i) + \partial_{x_j}(\rho U_i U_j) + \partial_{x_j}(\rho R_{ij}^L) = \rho g_i + \rho \left\langle U_{r,i}/\tau_p \right\rangle^L \end{array} \tag{2}$$

We emphasize that, by construction, the Reynolds stress tensor $\underline{\underline{R}}_{ij}^L$ complies with the so-called *realisability condition* (see [20, 24]):

$$\underline{x}^t \underline{\underline{R}}^L \underline{x} \geq 0 \tag{3}$$

for all $\underline{x} \in \mathscr{R}^2$.

Before going further on, we also mention that a time-splitting strategy is applied to system (2), which means that approximations of unsteady solutions of system (2) are obtained by solving successively an homogeneous evolution system:

$$\begin{array}{l} \partial_t \rho + \partial_{x_j}(\rho U_j) = 0 \\ \partial_t(\rho U_i) + \partial_{x_j}(\rho U_i U_j) + \partial_{x_j}(\rho R_{ij}^L) = 0 \end{array} \tag{4}$$

and then taking source terms into account, with frozen densities:

$$\begin{array}{l} \partial_t \rho = 0 \\ \partial_t(\rho U_i) = \rho g_i + \rho \left\langle U_{r,i}/\tau_p \right\rangle^L \end{array} \tag{5}$$

The present paper is organised as follows. In section 1, we propose two forms of the relaxation system associated with (4) that are quite similar. Then we discuss properties of both approaches in section 2, including some stability results. The last section is devoted to some two-dimensional numerical results.

1 Two distinct relaxation systems

In order to obtain approximate solutions of system (4) with non-smooth external data $\underline{\underline{R}}^L_{ij}$, we first introduce new variables $\underline{\underline{R}}_{ij}$ that are expected to relax towards $\underline{\underline{R}}^L_{ij}$ when some given relaxation time scale τ^R_p tends to 0. Since the tensor $\underline{\underline{R}}^L_{ij}$ is symmetric by construction, its counterpart $\underline{\underline{R}}_{ij}$ is also assumed to be symmetric. Hence, we need to introduce new partial differential equations that will govern the evolution of the Reynolds stresses $\underline{\underline{R}}_{ij}$.

This should be achieved in such a way that the new relaxation system were hyperbolic and would preserve the realizability of solutions, which means that $\underline{\underline{R}}_{ij}$ should comply with (3).

On the basis of [2, 16, 17], while introducing invariants II and I^L as defined below:

$$I^L = R^L_{ii} \quad and: \quad II = R_{ik}R_{ki} \tag{6}$$

the following relaxation system (7) naturally arises:

$$\begin{array}{l} \partial_t \rho + \partial_{x_j}(\rho U_j) = 0 \\ \partial_t(\rho U_i) + \partial_{x_j}(\rho U_i U_j) + \partial_{x_j}(\rho R_{ij}) = 0 \\ \partial_t(\rho R_{ij}) + \partial_{x_k}(\rho U_k R_{ij}) + \rho(R_{ik}\partial_{x_k}U_j + R_{jk}\partial_{x_k}U_i) = \rho\,\phi_{ij}/(\tau^R_p) \end{array} \tag{7}$$

noting :

$$\phi_{ij} = R_{ik}(R^L_{kl} - R_{kl})R_{lj}/I^L/(II)^{1/2}$$

with a classical Einstein summation notation for k,l. In the present work, the time scale τ^R_p is expected to be infinitely small. The differential part on the left hand side of (7) arises from the classical construction of motion of second-moment closures (see [1, 2, 13, 20, 23, 22, 24] among others). The non conservative terms $\rho(R_{ik}\partial_{x_k}U_j + R_{jk}\partial_{x_k}U_i)$ are usely -and abusively- called the production terms in the turbulent literature. These are actually convective contributions, and should be handled as such (see [1, 2, 4, 13]).

A first important point that is worth being mentionned is that the structure of the third equation in (7) guarantees the realisability of smooth solutions R_{ij}. The proof is rather simple. Introducing the determinant δ_R of the Reynolds stress tensor $\underline{\underline{R}}_{ij}$, which is precisely the product of the eigenvalues of $\underline{\underline{R}}_{ij}$, noting :

$$H_{ik} = R_{il}(R^L_{lk} - R_{lk})/(2I^L)/(II)^{1/2}/(\tau^R_p) - \partial_{x_k}U_i \tag{8}$$

and taking into account the mass balance equation (that is the first equation in (7)), we can rewrite the third equation of (7) as follows:

$$\partial_t(R_{ij}) + U_k\partial_{x_k}(R_{ij}) = H_{ik}R_{kj} + H_{jk}R_{ki} \tag{9}$$

Hence, we get the governing equation for δ_R (see [14, 15] for instance):

$$\partial_t(\delta_R) + U_k \partial_{x_k}(\delta_R) = 2H_{ll}\delta_R \tag{10}$$

which implies that, for positive initial conditions and inlet boundary conditions for δ_R, and assuming bounded values of the velocity U_k, its divergence $\partial_{x_k}(U_k)$ and the trace H_{ll}, smooth solutions $\delta_R(\mathbf{x},t)$ of equation (10) remain positive for $t \in [0,T]$, using a classical positivity lemma.

We focus now on the homogeneous part of system (7), thus concentrating on the evolution part of the relaxation system.

$$\begin{array}{l} \partial_t \rho + \partial_{x_j}(\rho U_j) = 0 \\ \partial_t(\rho U_i) + \partial_{x_j}(\rho U_i U_j) + \partial_{x_j}(\rho R_{ij}) = 0 \\ \partial_t(\rho R_{ij}) + \partial_{x_k}(\rho U_k R_{ij}) + \rho(R_{ik}\partial_{x_k} U_j + R_{jk}\partial_{x_k} U_i) = 0 \end{array} \tag{11}$$

1.1 A nonlinear interface relaxation system

System (11) is invariant under frame rotation, and it is also contains only one non-objective term corresponding to the non-conservative terms (see [24]). In order to define our interface solvers, we consider the reference frame $(\underline{n},\underline{\tau})$: $\underline{n} = (n_x, n_y)$, $\underline{\tau} = (-n_y, n_x)$, such that $n_x^2 + n_y^2 = 1$, for a given interface whose normal is $\underline{n}$. In practice, this interface will correspond to the interface separating two adjacent cells in the computational domain. We also introduce normal and tangential velocities U_n, U_τ, and components of the Reynolds stress tensor in the new reference frame $\mathbf{n}, \tau$:

$$\begin{array}{l} U_n = \underline{U}.\underline{n}, \\ U_\tau = \underline{U}.\underline{\tau}, \\ R_{nn} = \underline{n}^t.\underline{\underline{R}}.\underline{n}, \\ R_{n\tau} = \underline{n}^t.\underline{\underline{R}}.\underline{\tau} = \underline{\tau}^t\underline{\underline{R}}.\underline{n} = R_{\tau n}, \\ R_{\tau\tau} = \underline{\tau}^t.\underline{\underline{R}}.\underline{\tau}. \end{array} \tag{12}$$

Eventually, we define a normalized determinant called S:

$$S = \left((R_{nn})(R_{\tau\tau}) - (R_{n\tau})^2\right)/\rho^2 \tag{13}$$

together with a "non-conservative" variable:

$$Z^t = (\rho, U_n, U_\tau, \rho R_{nn}, \rho R_{n\tau}, S) \tag{14}$$

When neglecting transverse variations, thus assuming that $\forall\phi$, we have:

$$\partial\phi/\partial\tau = 0$$

and the relaxation system corresponding to system (11) written in terms of the new variable Z takes the following form for smooth solutions of (11):

$$\partial_t Z + A_n(Z)\partial_n Z = 0, \tag{15}$$

The exact expression of the matrix $A_n(Z)$ is given by:

$$A_n(Z) = \begin{pmatrix} U_n & \rho & 0 & 0 & 0 & 0 \\ 0 & U_n & 0 & \vartheta & 0 & 0 \\ 0 & 0 & U_n & 0 & \vartheta & 0 \\ 0 & \Psi_{nn} & 0 & U_n & 0 & 0 \\ 0 & 2\rho R_{n\tau} & \Phi_{n\tau} & 0 & U_n & 0 \\ 0 & 0 & 0 & 0 & 0 & U_n \end{pmatrix} \tag{16}$$

noting as usual the covolume $\vartheta(x,t) = 1/\rho(x,t)$, and setting:

$$\Psi_{nn} = 3\rho R_{nn}, \qquad \Phi_{n\tau} = \rho R_{nn}. \tag{17}$$

This approach (**R1**) corresponds to the approach introduced in [17]. Properties of system (15, 16, 17) will be detailed in section 2.

1.2 A true interface relaxation system

Rather than solving the one-dimensional Riemann problem in the n direction, on the basis of the previous system (15, 16), together with (17), the following approximation (18) is considered instead of (17):

$$\Psi_{nn} = 3A_0\vartheta, \qquad \Phi_{n\tau} = A_0\vartheta. \tag{18}$$

where : $A_0 = \rho_0^2(R_{nn})_0$, where $(R_{nn})_0 > 0$. This approach (**R2**) is actually a straightforward extension of the approach introduced in [10].

2 Main properties of relaxation systems R1, R2

We examine now the two systems connected with approaches **R1** and **R2** ; more precisely, we wish to detail the structure of the solution of the one-dimensional Riemann problem in each case. This is of course mandatory in order to construct exact or approximate interface Riemann solvers. We also wonder whether this solution -if any- complies with the realizability constraint -or not-.

2.1 Non-linear relaxation system R1

Before going further on, we need to define two celerities c_1, c_2 as follows:

$$c_1^2 = 3R_{nn} \quad \textit{and:} \quad c_2^2 = R_{nn} \tag{19}$$

We thus get:

Property 1:
System (15, 16) with closure (17) admits six real eigenvalues that read:

$$\lambda_{1,6} = U_n \pm c_1, \quad \lambda_{2,5} = U_n \pm c_2, \quad \lambda_3 = \lambda_4 = U_n, \tag{20}$$

Fields associated with eigenvalues $\lambda_{1,6}$ are genuinely non linear. Other fields are linearly degenerate.

Proof: The reader is refered to [17] for proof. As it occurs in the incompressible framework (see [14, 15]), eigenvalues are real if and only if the realizability constraint is fulfilled.

Due to the occurence of non-conservative products that are active in GNL fields, we must introduce *approximate* jump conditions in order to examine solutions of the associated one-dimensional Riemann problem (see [19]). For that purpose, we fix the following relations through discontinuities travelling at speed σ and separating two states Z_l, Z_r :

$$\begin{array}{l}
-\sigma\left[\rho\right] + \left[\rho U_n\right] = 0 \\
-\sigma\left[\rho U_n\right] + \left[\rho U_n^2 + \rho R_{nn}\right] = 0 \\
-\sigma\left[\rho U_\tau\right] + \left[\rho U_n U_\tau + \rho R_{n\tau}\right] = 0 \\
-\sigma\left[\rho R_{nn}\right] + \left[\rho U_n R_{nn}\right] + 2\left(\overline{\rho R_{nn}}\right)\left[U_n\right] = 0 \\
-\sigma\left[\rho R_{n\tau}\right] + \left[\rho U_n R_{n\tau}\right] + \left(\overline{\rho R_{nn}}\right)\left[U_\tau\right] + \left(\overline{\rho R_{n\tau}}\right)\left[U_n\right] = 0 \\
-\sigma\left[\rho R_{\tau\tau}\right] + \left[\rho U_n R_{\tau\tau}\right] + 2\left(\overline{\rho R_{n\tau}}\right)\left[U_\tau\right] = 0
\end{array} \tag{21}$$

where we note as usual $[\phi] = \phi_r - \phi_l$, and also $\overline{\phi} = (\phi_r + \phi_l)/2$, whatever ϕ is.

Moreover, we get the form of Riemann invariants after some calculations:

Property 2 (Riemann invariants in system associated with **R1**):
Denoting I_R^k the list of Riemann invariants associated with field k, we get:

$$
\begin{aligned}
I_R^1 &= \left\{ S, \tfrac{R_{nn}}{\rho^2}, \tfrac{R_{n\tau}}{\rho^2}, U_n + c_1, U_\tau + R_{n\tau}\tfrac{\sqrt{3}}{c_2} \right\} \\
I_R^2 &= \left\{ \rho, U_n, \rho R_{nn}, S, U_\tau + \tfrac{R_{n\tau}}{c_2} \right\} \\
I_R^{3,4} &= \{ U_n, U_\tau, \rho R_{nn}, \rho R_{n\tau} \} \\
I_R^5 &= \left\{ \rho, U_n, \rho R_{nn}, S, U_\tau - \tfrac{R_{n\tau}}{c_2} \right\} \\
I_R^6 &= \left\{ S, \tfrac{R_{nn}}{\rho^2}, \tfrac{R_{n\tau}}{\rho^2}, U_n - c_1, U_\tau - R_{n\tau}\tfrac{\sqrt{3}}{c_2} \right\}
\end{aligned}
\tag{22}
$$

Proof: The reader is refered to [17] for proof.

Therefore, we obtain the following result:

Property 3 (Existence and Uniqueness of the solution of the Riemann problem for R1):
The Riemann problem associated with (15, 16,17), approximate jump relations (21), and realizable initial conditions for left and right states Z_L, Z_R, admits a unique solution with no vacuum occurence if:

$$
(U_n)_R - (U_n)_L < \sqrt{3}\left(\sqrt{(R_{nn})_L} + \sqrt{(R_{nn})_R} \right). \tag{23}
$$

The solution is composed of six constant states $Z_L, Z_1, Z_2, Z_3, Z_4, Z_R$ separated by 2 GNL waves associated with $\lambda_{1,6}$ and 4 LD waves associated with $\lambda_{2,3,4,5}$. All intermediate states arising in the solution of the one-dimensional Riemann problem comply with the realizability condition (3).

Proof: The reader is refered to [17] for proof.

Actually, we emphasize that the 2 and 5 fields are ghost waves for the three components ρ, U_n, R_{nn}. This explains why the condition of existence and uniqueness of the approximate solution is exactly the same as in the pure one-dimensional framework. We also note that S is a Riemann invariant in the $1,2,5,6$ waves; besides, the approximate jump conditions (21) are such that $[S] = 0$, thus S satisfies some maximum principle : $min(S_L, S_R) \leq S(x_n/t) \leq max(S_L, S_R)$.

However, as occurs in the one-dimensional case, the validity of *a priori* jump conditions (21) is questionable. Hence it seems natural to introduce a

slightly modified version of the approach (**R1**), which consists in replacing closure (17) by (18). This one is analyzed in detail below.

2.2 Relaxation system R2

We turn now to **R2** and we introduce:

$$(\tilde{c}_1)^2 = 3A_0\vartheta^2 \quad \textit{and:} \quad (\tilde{c}_2)^2 = A_0\vartheta^2 \tag{24}$$

and get:

Property 4:
Assume that $0 \leq \rho$ *; then system (15, 16) with closure (18) admits six real eigenvalues that read:*

$$\tilde{\lambda}_{1,6} = U_n \pm \tilde{c}_1, \quad \tilde{\lambda}_{2,5} = U_n \pm \tilde{c}_2, \quad \tilde{\lambda}_3 = \lambda_4 = U_n, \tag{25}$$

All fields are linearly degenerate.

The proof is straightforward and is left to the reader. The determinant of $A_n(Z) - \tilde{\lambda}\mathscr{I}$ is:

$$det(A_n(Z) - \tilde{\lambda}\mathscr{I}) = (W_n)^2((W_n)^2 - \vartheta\Phi_{n\tau})((W_n)^2 - \vartheta\Psi_{nn})$$

where $W_n = U_n - \tilde{\lambda}$. This provides in a straightforward way the expression of eigenvalues. Thus, it only remains to check that :

$$\nabla_Z\tilde{\lambda}_k(Z).\tilde{r}_k(Z) = 0$$

where $\tilde{r}_k(Z)$ stands for the right eigenvector associated with the eigenvalue $\tilde{\lambda}_k$, whatever k is. Starting from (16), the complete list of right eigenvectors $\tilde{r}_k(Z)$ of $A_n(Z)$ may be written in the general case:

$$\begin{array}{l}
\tilde{r}_1 = (\rho, -c_1, \frac{-2\rho c_1 R_{n\tau}}{\rho c_1^2 - \Phi_{n\tau}}, \rho c_1^2, \frac{\rho c_1^2}{\rho c_1^2 - \Phi_{n\tau}}, 0) \\
\tilde{r}_2 = (0, 0, 1, 0, -\rho c_2, 0) \\
\tilde{r}_3 = (1, 0, 0, 0, 0, 0) \\
\tilde{r}_4 = (0, 0, 0, 0, 0, 1) \\
\tilde{r}_5 = (0, 0, 1, 0, \rho c_2, 0) \\
\tilde{r}_6 = (\rho, c_1, \frac{2\rho c_1 R_{n\tau}}{\rho c_1^2 - \Phi_{n\tau}}, \rho c_1^2, \frac{\rho c_1^2}{\rho c_1^2 - \Phi_{n\tau}}, 0)
\end{array} \tag{26}$$

where $\Phi_{n\tau} = A_0\vartheta$ when focusing on **R2**.

Unlike in the previous case (**R1**) where approximate jump conditions were prescribed, the connection between two states separated by a contact

discontinuity is uniquely defined, and it only requires giving Riemann invariants through all fields. When looking for $f_k(Z)$ such that:

$$\nabla_Z f_k(Z).\tilde{r}_k(Z) = 0$$

we obtain the counterpart of property 2 which is now:

Property 5 (Riemann invariants in system associated with **R2**):
Riemann invariants associated with (15, 16,18) are the following:

$$\begin{aligned}
\tilde{I}_R^1 &= \left\{ S, \rho R_{nn} + 3A_0\vartheta, \tfrac{R_{n\tau}}{\rho^2}, U_n - a_0\vartheta, U_\tau + \tfrac{\rho R_{n\tau}}{a_0} \right\} \\
\tilde{I}_R^2 &= \left\{ \rho, U_n - \sqrt{A_0}\vartheta, \rho R_{nn}, S, U_\tau + \tfrac{R_{n\tau}}{\tilde{c}_2} \right\} \\
\tilde{I}_R^{3,4} &= \{ U_n, U_\tau, \rho R_{nn}, \rho R_{n\tau} \} \\
\tilde{I}_R^5 &= \left\{ \rho, U_n + \sqrt{A_0}\vartheta, \rho R_{nn}, S, U_\tau - \tfrac{R_{n\tau}}{\tilde{c}_2} \right\} \\
\tilde{I}_R^6 &= \left\{ S, \rho R_{nn} + 3A_0\vartheta, \tfrac{R_{n\tau}}{\rho^2}, U_n + a_0\vartheta, U_\tau - \tfrac{\rho R_{n\tau}}{a_0} \right\}
\end{aligned} \tag{27}$$

setting $a_0 = \sqrt{3A_0}$.

We may then construct the whole solution of the one-dimensional Riemann problem, which is rather easy since the connection through waves is uniquely defined by the Riemann invariant parametrization. We may give the following result:

Property 6 (Existence and Uniqueness of the solution of the Riemann problem for **R2**).
Assume that $\rho_0^2(R_{nn})_0 \geq 0$ *is such that it satisfies the Wave Ordering Condition (WOC):*

$$\tilde{\lambda}_1 < \tilde{\lambda}_2 < \tilde{\lambda}_3 = \tilde{\lambda}_4 < \tilde{\lambda}_5 < \tilde{\lambda}_6. \tag{28}$$

Then the Riemann problem associated with (15), (18) and initial conditions Z_L, Z_R *satisfying (3), admits a unique solution composed of six constant states* $Z_L, \tilde{Z}_1, \tilde{Z}_2, \tilde{Z}_3, \tilde{Z}_4, Z_R$ *separated by six LD waves. These are such that:*

$$\tilde{\rho}_1 = \tilde{\rho}_2 > 0 \qquad \tilde{\rho}_3 = \tilde{\rho}_4 > 0$$

and also:

$$\tilde{S}_1 = \tilde{S}_2 > 0 \qquad \tilde{S}_3 = \tilde{S}_4 > 0$$

The proof is obtained by construction. The normal component of the velocity is unique:

$$(\tilde{U_n})_1 = (\tilde{U_n})_2 = (\tilde{U_n})_3 = (\tilde{U_n})_4 = \tilde{U_n} \tag{29}$$

where:

$$\tilde{U_n} = ((U_n)_L + (U_n)_R)/2 - ((\rho R_{nn})_R - (\rho R_{nn})_L)/(2a_0)$$

We also note that the component ρR_{nn} is unique since:

$$(\tilde{\rho}\tilde{R}_{nn})_1 = (\tilde{\rho}\tilde{R}_{nn})_2 = (\tilde{\rho}\tilde{R}_{nn})_3 = (\tilde{\rho}\tilde{R}_{nn})_4 = \Pi \tag{30}$$

where:

$$\Pi = ((\rho R_{nn})_R + (\rho R_{nn})_L)/2 - a_0((U_n)_R - (U_n)_L)/2$$

Obviously, Π is positive provided that initial conditions are such that:

$$(U_n)_R - (U_n)_L < ((\rho R_{nn})_L + (\rho R_{nn})_R)/a_0 \tag{31}$$

which should be compared with the condition of existence and uniqueness of the solution with no vacuum occurence to the Riemann problem associated with **R1** in (23). The condition (31) may be violated in strong rarefaction waves. Intermediate values of the density are given by:

$$\begin{array}{l} \tilde{\vartheta_1} = \vartheta_L + ((U_n)_R - (U_n)_L - ((\rho R_{nn})_R - (\rho R_{nn})_L)/a_0)/(2a_0) \\ \tilde{\vartheta_3} = \vartheta_R + ((U_n)_R - (U_n)_L + ((\rho R_{nn})_R - (\rho R_{nn})_L)/a_0)/(2a_0) \end{array} \tag{32}$$

The WOC condition implies that :

$$\tilde{\lambda}_1 < \tilde{\lambda}_3 = \tilde{\lambda}_4 < \tilde{\lambda}_6$$

which guarantees positive values of densities $\tilde{\rho}_1$ and $\tilde{\rho}_3$ (see [10]). It only remains to check that: $\tilde{\lambda}_1 < \tilde{\lambda}_2 < \tilde{\lambda}_3$, which is quite obvious since:

$$\tilde{\lambda}_1 = (\tilde{U_n})_1 - \tilde{c}_1 = U_n - a_0\tilde{\vartheta_1} < U_n - \sqrt{A_0}\tilde{\vartheta_1} = \tilde{\lambda}_2 < U_n = \tilde{\lambda}_3 = \tilde{\lambda}_4$$

A similar result holds on the right hand side of the central wave associated with U_n.

We also emphasize that components U_τ and $\rho R_{n\tau}$ do not vary through the central wave associated with the eigenvalue $\lambda_3 = \lambda_4 = U_n$; concerning U_τ, this basically differs from what happens in a compressible laminar framework.

Components $R_{\tau\tau}$ are calculated using the identity:

$$R_{\tau\tau} = (\rho^2 S + (R_{n\tau})^2)/R_{nn}$$

Hence $R_{\tau\tau}$ is positive if and only if R_{nn} is positive. The normalized determinant S is positive since:

$$\tilde{S}_1 = \tilde{S}_2 = S_L > 0 \quad and \quad \tilde{S}_3 = \tilde{S}_4 = S_R > 0$$

Details on intermediate states $U_\tau, R_{n\tau}$ are given in appendix A.

Property 6 was more or less expected, for readers who are familiar with turbulent compressible models.

Eventually, we wish to emphasize that the WOC is the same as in the pure one-dimensional framework (see [6, 10]), and we only briefly recall it in appendix A.

2.3 Stability properties

We focus on the evolution step in the relaxation procedure, and thus on the homogeneous system corresponding to the left hand side of (7), in a two-dimensional framework, restricting to smooth solutions $\rho(\underline{x},t)$, $U_i(\underline{x},t)$, $R_{ij}(\underline{x},t) \in \mathscr{C}^1$. We denote by

$$\mathscr{E}_1(t) = \frac{1}{2}\int_\Omega \rho U_i^2(\underline{x},t)d\Omega \quad \text{and} \quad \mathscr{E}_2(t) = \frac{1}{2}\int_\Omega \rho\ tr(\underline{\underline{R}})(\underline{x},t)d\Omega, \quad i = 1,2. \tag{33}$$

the kinetic energy of the mean motion and the energy of the fluctuating particle motion respectively. The total particle energy is given by

$$\mathscr{E}(t) = \mathscr{E}_1(t) + \mathscr{E}_2(t).$$

We also assume wall-boundary conditions on the boundary of the domain, that is: $\forall \underline{x} \in \partial\Omega \quad \underline{U}.\underline{n} = 0$ and $\underline{\underline{R}}\underline{n} = \underline{0}$.

Property 7.
We assume that $S(\underline{x} \in \partial\Omega, t > t_0) > 0$ on the boundary, and also that the initial condition is such that $S(\underline{x} \in \Omega, t_0) > 0$. *Then smooth solutions of the homogeneous relaxation system corresponding to the left-hand side of system (7) satisfy the following estimate:*

$$0 \leq \mathscr{E}_1(t) = \mathscr{E}(t_0) - \mathscr{E}_2(t) \leq \mathscr{E}(t_0), \tag{34}$$

since $\mathscr{E}_2(t) \geq 0$

Proof: Starting from (7)), and using the mass balance equation, we easily obtain that smooth solutions comply with:

$$\partial_t(\rho U_l U_l/2) + \partial_{x_j}(\rho U_l U_l U_j/2) + U_l \partial_{x_j}(\rho R_{lj}) = 0$$

but also:

$$\partial_t(\rho R_{ll}) + \partial_{x_k}(\rho U_k R_{ll}) + 2\rho R_{lk}\partial_{x_k} U_l = 0$$

and thus:

$$\partial_t(\frac{\rho(U_l U_l + R_{ll})}{2}) + \partial_{x_k}(U_k(\frac{\rho(U_l U_l + R_{ll})}{2}) + \rho U_l R_{lk}) = 0$$

Adding the latter two equations, integrating over the whole domain Ω , using definitions (33), and taking wall boundary conditions into account on $\partial\Omega$, we get at once:

$$\partial_t(\mathscr{E}(t)) + \int_{\partial\Omega}((\frac{\rho(U_l U_l + R_{ll})}{2})U_k n_k + \rho U_l R_{lk} n_k) d\sigma = 0$$

and eventually:

$$\partial_t(\mathscr{E}(t)) = 0$$

which means that : $\mathscr{E}(t) = \mathscr{E}(0)$ at any time $t > 0$. Furthermore, as it has been emphasized in section 1, the governing equation of S is:

$$\partial_t S + (\underline{U} \cdot \nabla S) = 0. \tag{35}$$

Integrating along smooth characteristic lines, and owing to relevant initial and boundary conditions on S, we may conclude that the eigenvalues remain positive, which in turn provides: $R_{ll}(\underline{x},t) > 0$, since R_{ll} corresponds with the sum of eigenvalues of $\underline{\underline{R}}$. Thus : $\mathscr{E}_2(t) > 0$. On the whole, we may conclude that for $t > 0$:

$$0 \leq \mathscr{E}_1(t) \leq \mathscr{E}(t_0)$$

We emphasize here that this result cannot be obtained directly, using the sole mass balance and mean momentum equations. Moreover, there is no need to use a gradient-type closure law for Reynolds stresses in order to obtain this result, as it is sometimes argued. Of course, viscous -or other dissipative- effects might be added in the mean momentum equation ; these would result in a strict dissipation of the whole kinetic energy of the mean motion. Other boundary conditions may be taken into account.

3 Numerical algorithm

In order to compute the approximations of solutions of system (2) at each time step, the Finite Volume method relies on a classical fractional step method, which proceeds in three distinct steps:

- An evolution step;
- An instantaneous relaxation step;
- A physical step to take sources into account.

3.1 Algorithm

The whole algorithm is thus the following:

• **Step 1 (Evolution):**
Starting from the conservative variable W_i^n:

$$W_i^n = (\rho^n, (\rho U_i)^n, (\rho R_{ij})^n)$$

compute approximate solutions:

$$W_i^{n+1,-} = (\rho^{n+1,-}, (\rho U_i)^{n+1,-}, (\rho R_{ij})^{n+1,-})$$

of the homogeneous system corresponding to the left hand side of (7) at time t^{n+1}, using an approximate Godunov solver for (**R1**) (see [17]) or a relaxation interface solver for (**R2**).

• **Step 2 (Relaxation):**
Restore local values of the Reynolds stresses $R_{ij} = R_{ij}^L$:

$$\rho^{n+1} = \rho^{n+1,-}, \quad (\rho U_i)^{n+1} = (\rho U_i)^{n+1,-}, \quad (\rho R_{ij})^{n+1} = \rho^{n+1}(R_{ij}^L)^{n+1}.$$

• **Step 3 (Sources):**
Account for physical source terms (right hand side of (2)).

We describe now the Finite Volume algorithm that is used in order to obtain numerical approximations of solutions of the evolution step.

3.2 Evolution step

We introduce a partition of the computational domain in non-overlapping cells Ω_i, the measure of which is $vol(\Omega_i)$. The surface separating two adjacent cells i and j is S_{ij}, the outward normal vector n_{ij} pointing from cell i to cell j. We denote $V(i)$ the set of neighbouring cells of Ω_i. A time step Δt^n is

obtained using a classical CFL-like condition. At each time step, the scheme computes approximate values W_i^n of $\int_{\Omega_i} W(\underline{x},t^n)d\omega/vol(\Omega_i)$, using the rule:

$$\begin{array}{rl} vol(\Omega_i)(\rho_i^{n+1}-\rho_i^n)+\Delta t^n & \Sigma_{j\in V(i)}\left((\rho^*\underline{U}^*\cdot\underline{n})_{ij}S_{ij}\right)=0 \\ vol(\Omega_i)((\rho\underline{U})_i^{n+1}-(\rho\underline{U})_i^n)+\Delta t^n & \Sigma_{j\in V(i)}\left((\rho^*\underline{U}^*(\underline{U}^*\cdot\underline{n}))_{ij}S_{ij}\right) \\ +\Delta t^n & \Sigma_{j\in V(i)}\left((\rho^*\underline{\underline{R}}^*\underline{n}))_{ij}S_{ij}\right)=0 \end{array} \quad (36)$$

We use here the convention that:

$$(\phi^*)_{ij}=\phi^{Riemann}(W_L=W_i^n,W_R=W_j^n,\underline{n}_{ij};\frac{x_n-(x_n)_{ij}}{t}=0)$$

where the solution of the one-dimensional Riemann problem corresponds to approach **R2** (or **R1**) in the x_n direction.

4 Numerical results

An extensive validation of both methods **(R1, R2)** has been achieved in [11] in the one-dimensional framework, by computing the L^1 norm of the error for analytical solutions of Riemann problems associated with the homogeneous part of (2), assuming specific forms for $R^L_{ij} = r_{ij}(\rho, U)$. One important conclusion in the latter reference was that rather small discrepancies between **(R1)** and **(R2)** were observed in all computations investigated ; another essential point was that both of them could handle shock computations, which was expected due to the conservative form of the relaxed system (4). Thus we only show here a few two-dimensional noisy computations and we put emphasis on the main conclusions.

4.1 A two-dimensional shock tube with noise

We start with a two-dimensional test case where the form of Lagrangian stress tensor $\underline{\underline{R}}^L$ is synthetic. The exact values are given by:

$$R^L_{ij}(\underline{x},t) = R_0 \rho^{\gamma-1} \left(1 + RMS(0.5 - random(0,1))\right) \delta_{ij}$$

with $\gamma = 3$, $R_0 = 10^5$, $RMS = 0.5$. The value of RMS enables to fix the noise amplitude. Obviously solutions may no longer be spherical, even when the initial condition is invariant under rotation.

The regular mesh contains 10^4 squares, and the CFL number is set to 0.5. The initial conditions for the mean values ρ and U are the following.

If $x + y < 0$, we set:

$$\rho(\underline{x}, t = 0) = 1 \quad U_x(\underline{x}, t = 0) = U_y(\underline{x}, t = 0) = 0$$

Otherwise, for $x + y > 0$, we set:

$$\rho(\underline{x}, t = 0) = 0.35 \quad U_x(\underline{x}, t = 0) = U_y(\underline{x}, t = 0) = 0$$

All boundary conditions are left free, using a discrete homogeneous Neumann approach for states on both sides of boundary interfaces.

Hence oblique rarefaction waves and shock waves propagate parallel to the direction $y = x$, and, when restricting to the density contours (see figure 1), we retrieve an important smoothing effect of noise, though the value of RMS is rather high here, especially close to the shock structure. We may conjecture that both the non-linear pattern of the set of PDE, and the stabilization due to the upwinding scheme contribute to this pattern. Of course, the mesh is rather coarse here, which emphasizes the smoothing effect.

Details on the effect of *RMS* values on solutions are available in [11], together with classical studies of mesh refinement.

4.2 A two-dimensional collapse over a moving fluid

The second case we consider corresponds to the collapse of a fluid structure plunged in a uniform moving frame. We use again a synthetic isotropic signal:

$$R_{ij}^L(\underline{x},t) = R_0 \rho^{\gamma-1} \left(1 + RMS(0.5 - random(0,1))\right) \delta_{ij}$$

with the same values of parameters as defined above. The initial condition for ρ, U is as follows:

- If $(x-x_0)^2 + (y-y_0)^2 < r_0^2$, we set:

$$\rho(\underline{x},t=0) = 1 \quad \rho U_x(\underline{x},t=0) = 100 \quad \rho U_y(\underline{x},t=0) = 0$$

- Otherwise, for: $(x-x_0)^2 + (y-y_0)^2 > r_0^2$, we set:

$$\rho(\underline{x},t=0) = 0.35 \quad \rho U_x(\underline{x},t=0) = 290 \quad \rho U_y(\underline{x},t=0) = 0$$

with $(x_0, y_0) = (0,0)$, $r_0 = 0.1$ and $\Omega = [-0.5, 0.5]^2$. Hence there is a slip in the initial condition at the bottom of the circular region $(x-x_0)^2 + (y-y_0)^2 < r_0^2$. Values of RMS are uniform and equal to $RMS = 0.5$ in the region $0 < (x-x_0)^2 + (y-y_0)^2 < r_1^2$ with $r_1 = \sqrt{2}/2$.

The first mesh contains 1000×100 rectangular uniform cells. Figures 2 give the contours of the density at times $t = 0$ and $t = 4 \times 10^{-4}$. We may observe the "wall" effects around the surface travelling at a smaller speed, which result in a local increase of the density. This relative speed effect is superimposed to the collapsing effect. Profiles of the density are also available in figure 4, at two different times $t = T_1 = 5 \times 10^{-5}$ and $t = T_2 = 4 \times 10^{-4}$, together with ρU and the R_{xx} component. ; one can observe strong oscillations connected with the noise contribution, especially in almost uniform regions. A strong rarefaction wave develops behind the collapse, which was expected, and its perturbation by the synthetic Reynolds tensor tends to vanish as the mean density tends to zero, and then increases again when ρ increases.

Figures 3 show the norm of the particle velocity field. Though the structures seem to be symmetric with respect to the line $y = 0$, we emphasize that it is not, owing to the random contributions. However, this can be hardly observed on figure 5 due to the post-processing.

Figures 5 provide the same density contours when the computational mesh is refined (the second mesh contains 4000×400 regular rectangles).

In addition, we provide the counterpart for density and x-velocity profiles along the vertical line $y = 0$ (see figure 7). The analysis of computational results becomes easier when looking at time evolutions in movies.

We again refer to [11] that examines in detail the influence of the mesh size on noisy calculations in a one-dimensional framework.

4.3 A highly anisotropic case

The third test case is quite similar except for the fact that the synthetic Reynolds stress tensor is highly anisotropic, since:

$$R_{ij}^L(\underline{x},t) = R_0 \rho^{\gamma-1} \left(1 + RMS(0.5 - random(0,1))\right) M_{ij}$$

with $\gamma = 3$, $R_0 = 10^5$, $RMS = 0.5$, and:

$$M_{xx} = 5/4, \quad M_{xy} = M_{yx} = 1/4, \quad M_{yy} = 3/4.$$

R_{ij}^L is symmetric positive definite unless a vacuum occurs in the solution. The initial condition for ρ, U is given below.

- If $(x-x_0)^2 + (y-y_0)^2 < 0.01$, we set:

$$\rho(\underline{x}, t=0) = 1$$

- Otherwise, we set:

$$\rho(\underline{x}, t=0) = 0.35$$

still using: $(x_0, y_0) = (0,0)$. The fluid is at rest at the beginning of the computation:

$$U_x(\underline{x}, t=0) = U_y(\underline{x}, t=0) = 0.$$

The computational domain is again: $\Omega = [-0.5, 0.5]^2$, and we use here a fine mesh including $1000x1000$ regular cells.

The structure of the solution is rather complex. Nonetheless we may retrieve the principal axes that are aligned with :

$$r_+ = (1, (1+\sqrt{2})^{-1}) \quad , \quad r_- = (1, (1-\sqrt{2})^{-1})$$

Moreover, the ratio of diameters of principal axes D/d of the ellipse is approximately equal to the following ratio c_+/c_- (see figure 8):

$$\frac{c_+}{c_-} = (\frac{\lambda_+}{\lambda_-})^{1/2} (\rho_+/\rho_-)^{(\gamma-1)/2}$$

where ρ_+ (respectively ρ_-) stands for the value of the mean density just before the shock propagating in the r_+ (respectively r_-) direction, and also noting $\lambda_\pm$ the eigenvalue associated with the right eigenvector $r_\pm$:

$$\lambda_\pm = 1 \pm (2\sqrt{2})^{-1}$$

The low values of the mean density at the origin $(0,0)$ are due to the interaction and reflection of initial -anisotropic- rarefaction waves generated by the initial discontinuity of the mean density at $r = 0.1.$.

Conclusion

We have presented in this paper a new relaxation technique **R2**, and the main properties of the former approach **R1** and of the new one **R2** have been detailed. It has been shown that the stability of the relaxation system is such that the kinetic energy of the mean momentum remains bounded in the Eulerian approach. Some two-dimensional results have been discussed, and we refer to the reference paper [11] where the mesh refinement effects have been investigated in detail.

Actually, when computing approximations of solutions of system 2, the relaxation technique **R2** provides a useful tool in order to compute approximate values of fluxes at each interface of the Finite Volume mesh. It does not require introducing approximate jump conditions in the Riemann problem for the relaxation system, unlike in the former relaxation approach **R1** (see [17]). The anisotropy of the Reynolds stress tensor R_{ij}^L may be taken into account, which is known to be mandatory for real computations involving fully-developped turbulence (see for instance appendix in [4] where some nice example of numerical instability is exhibited). The relaxation approach **R2** provides a rather nice stability of the whole algorithm. It may be conjectured that the conservative form of the scheme (36), which is in agreement with the conservative form of system (4), guarantees the convergence towards correct solutions of (4), even when shocks develop.

Eventually, we emphasize that this algorithm has been extensively used for the unsteady coupling of a Lagrangian code with its Eulerian counterpart, while focusing on the particle jet in a coaxial air flow along a wall boundary, as detailed in [9]. The extension of the relaxation approaches (**R1**) and (**R2**) to the three-dimensional framework is straightforward but rather technical.

Acknowledgements

The first author received a financial support through an EDF-CIFRE contract 203/2009. All computational facilities were provided by EDF.

Appendix A

- Wave ordering condition (WOC)
Intermediate states of density are positive if:

$$\begin{cases} 2\vartheta_l a_0^2 + [U_n]_l^r a_0 - [\rho R_{nn}]_l^r > 0 \\ 2\vartheta_r a_0^2 + [U_n]_l^r a_0 + [\rho R_{nn}]_l^r > 0 \end{cases} \tag{37}$$

We introduce :

$$\Delta_1 = ([U_n]_l^r)^2 + 8\vartheta_l [\rho R_{nn}]_l^r \qquad \Delta_2 = ([U_n]_l^r)^2 - 8\vartheta_r [\rho R_{nn}]_l^r. \tag{38}$$

If $\Delta_1 \geq 0$ we set:

$$(a_0)_{1,2} = \frac{-[U_n]_l^r \pm \sqrt{\Delta_1}}{4\vartheta_l}.$$

If $\Delta_2 \geq 0$, we set:

$$(a_0)_{3,4} = \frac{-[U_n]_l^r \pm \sqrt{\Delta_2}}{4\vartheta_r}.$$

Starting with a minimal value $a_{min} > 0$, a_0 must be chosen such that :
If $\Delta_1 \geq 0$ and $\Delta_2 \geq 0$ then a_0 should be greater than $max\left\{a_{min}, (a_0)_{i\in(1,2,3,4)}\right\}$
If $\Delta_1 \geq 0$ and $\Delta_2 < 0$ then a_0 should be greater than $max\left\{a_{min}, (a_0)_{i\in(1,2)}\right\}$
If $\Delta_1 < 0$ and $\Delta_2 \geq 0$ then a_0 should be greater than $max\left\{a_{min}, (a_0)_{i\in(3,4)}\right\}$.
If $\Delta_1 < 0$ and $\Delta_2 < 0$ then $a_0 > a_{min}$.

In practice, a_{min} is chosen such that:

$$a_{min} = max(\rho_l(|U_n| + c_1)_l, \rho_r(|U_n| + c_1)_r)$$

- Intermediate states U_τ and $R_{n\tau}$ in the one-dimensional Riemann problem associated with the relaxation system **R2**.

- Reynolds stress components $R_{n\tau}$:

$$(\tilde{\rho}\tilde{R}_{n\tau})_1 = (\rho R_{n\tau})_L (\vartheta_L/\vartheta_1)^3, \qquad (\tilde{\rho}\tilde{R}_{n\tau})_4 = (\rho R_{n\tau})_R (\vartheta_R/\vartheta_4)^3,$$

$$\begin{aligned}(\tilde{\rho}\tilde{R}_{n\tau})_2 = (\tilde{\rho}\tilde{R}_{n\tau})_3 = a_0/(2\sqrt{3})\left\{(U_\tau)_L - (U_\tau)_R + (\rho R_{n\tau}/a_0)_L + (\rho R_{n\tau}/a_0)_R\right\} \\ +(\sqrt{3}-1)\left[(\tilde{\rho}\tilde{R}_{n\tau}/a_0)_1 + (\tilde{\rho}\tilde{R}_{n\tau}/a_0)_4\right] a_0/(2\sqrt{3}),\end{aligned} \tag{39}$$

- Tangential Velocities U_τ:

$$(\tilde{U}_\tau)_1 = (U_\tau)_L + (\rho R_{n\tau})_L/a_0 - (\tilde{\rho}\tilde{R}_{n\tau})_1/a_0,$$

$$\begin{aligned}(\tilde{U}_\tau)_2 = (\tilde{U}_\tau)_3 = ((U_\tau)_L + (U_\tau)_R)/2 + ((\rho R_{n\tau})_L - (\rho R_{n\tau})_R)/2a_0 \\ + \left((\sqrt{3}-1)(\tilde{\rho}\tilde{R}_{n\tau})_1 + (1-\sqrt{3})(\tilde{\rho}\tilde{R}_{n\tau})_4\right)/2a_0,\end{aligned} \tag{40}$$

$$(\tilde{U}_\tau)_4 = (U_\tau)_R - (\rho R_{n\tau})_R/a_0 + (\tilde{\rho}\tilde{R}_{n\tau})_4/a_0.$$

References

[1] B. AUDEBERT, "Contribution à l'analyse de l'interaction onde de choc - couche limite", *Université Pierre et Marie Curie*, PhD thesis, 2006.

[2] C. BERTHON, F. COQUEL, J.M. HÉRARD AND M. UHLMANN, "An approximate solution of the Riemann problem for a realisable second-moment turbulent closure", *Shock Waves Journal*, vol. 11 (4), pp. 245-269, 2002.

[3] F. BOUCHUT, "Nonlinear stability of finite volume methods for hyperbolic conservation laws and well-balanced schemes for source", *Frontiers in Mathematics Series*, Birkhauser, 2004.

[4] G. BRUN, J.M. HÉRARD, D. JEANDEL AND M. UHLMANN, "An approximate Riemann solver for a class of realizable second order closures", *Int. J. of Comp. Fluid Dynamics*, vol. 13, n 3, pp. 223-249, 1999.

[5] C. CHALONS, F. COQUEL AND C. MARMIGNON, "Well-balanced time implicit formulation of relaxation schemes for the Euler equations", *SIAM J. Sci. Comput*, vol 30, issue 1, pp 394-415, 2007.

[6] C. CHALONS, J.F. COULOMBEL, "Relaxation approximation of the Euler equations", *J. Math. Anal. Appl.*, vol. 348, pp. 872-893, 2008.

[7] S. CHIBBARO, J.M. HÉRARD AND J.P. MINIER, "A novel Hybrid Moments/Moments-PDF method for turbulent two-phase flows", *Final Technical Report Activity Marie Curie Project. TOK project LANGE Contract MTKD-CT-2004 509849*, 2006.

[8] F. COQUEL, E. GODLEWSKI, SEGUIN, N., "Relaxation of fluid systems", *Mathematical Models and Methods in Applied Sciences*, DOI No: 10.1142/S0218202512500145, 2012.

[9] K. DOROGAN, "Schémas numériques pour la modélisation hybride des écoulements turbulents gaz-particules", *PhD thesis*, Université Aix Marseille, France, 2012.

[10] K. DOROGAN, M. GUINGO, J.M. HÉRARD, J.P. MINIER, "A relaxation scheme for hybrid modelling of gas-particle flows", *submitted for publication in revised form*.

[11] K. DOROGAN, J.M. HÉRARD, J.P. MINIER, "Development of a new scheme for hybrid modelling of gas-particle two-phase flows", *EDF report H-I81-2010-2352-EN*, 2010.

[12] R. EYMARD, T. GALLOUET AND R. HERBIN, "Finite Volume Methods", *Handbook of Numerical Analysis*, vol. VII, pp. 713-1020, 2000.

[13] S. GAVRILYUK, H. GOUIN, "Geometric evolution of the Reynolds stress tensor in three-dimensional turbulence", *European J. Mechanics B/Fluids, http://hal.archives-ouvertes.fr/hal-00371444/en/*, submitted, 2010.

[14] J.M. HÉRARD, "Basic analysis of some second-moment closures. Part II: incompressible turbulent flows including buoyant effects", *EDF report HE-41/93/37A*, 1993.

[15] J.M. HÉRARD, "Realizable non-degenerate second-moment closures for incompressible turbulent flows", *CRAS Paris IIb*, vol. 322, pp. 371-377, 1996.

[16] J.M. HÉRARD, "A relaxation tool to compute hybrid Euler-Lagrange compressible models", *AIAA paper 2006-2872, 36th AIAA FD Conference, http://www.aiaa.org*, 2006.

[17] J.M. HÉRARD, M. UHLMANN AND D.E. VAN DER VELDEN, "Numerical techniques for solving hybrid Eulerian-Lagrangian models for particulate flows", *EDF report H-I81-2009-3961-EN*, pp. 1-50, 2009 (unpublished).

[18] S. JIN AND Z. XIN, "The relaxation schemes for systems of conservation laws in arbitrary space dimensions", *Comm. Pure Appl. Math.*, vol 48, pp. 235-276, 1995.

[19] P.G. LE FLOCH, "Entropy weak solutions to non-linear hyperbolic systems in non-conservative form", *Comm. in Part. Diff. Eq.*, vol 13(6), pp. 669-727, 1988.

[20] J.L. LUMLEY, "Computational modelling of turbulent flows", *Advances in Applied Mechanics*, vol. 18, pp. 123-176, 1978.

[21] M. MURADOGLU, P. JENNY, S.B. POPE AND D.A. CAUGHEY, "A consistent hybrid finite-volume/particle method for the pdf equations of turbulent reactive flows", *Journal of Computational Physics*, vol. 154, pp. 342-371, 1999.

[22] S.B. POPE, "PDF methods for turbulent reactive flows", *Prog. Energy Comb. Sci.*, vol. 11, pp. 119-192, 1985.

[23] S.B. POPE, "On the relationship between stiochastic Lagrangian models of turbulence and second-moment closures", *Physics of Fluids*, vol. 6(2), pp. 973-985, 1984.

[24] U. SCHUMANN, "Realizability of Reynolds stress turbulent models", *Physics of Fluids*, vol. 20 (5), pp. 721, 1977.

[25] I. SULICIU, "On the thermodynamics of fluids with relaxation and phase transitions. Fluids with relaxation", *Internat. J. Engrg. Sci.*, vol. 36, pp. 921-947, 1998.

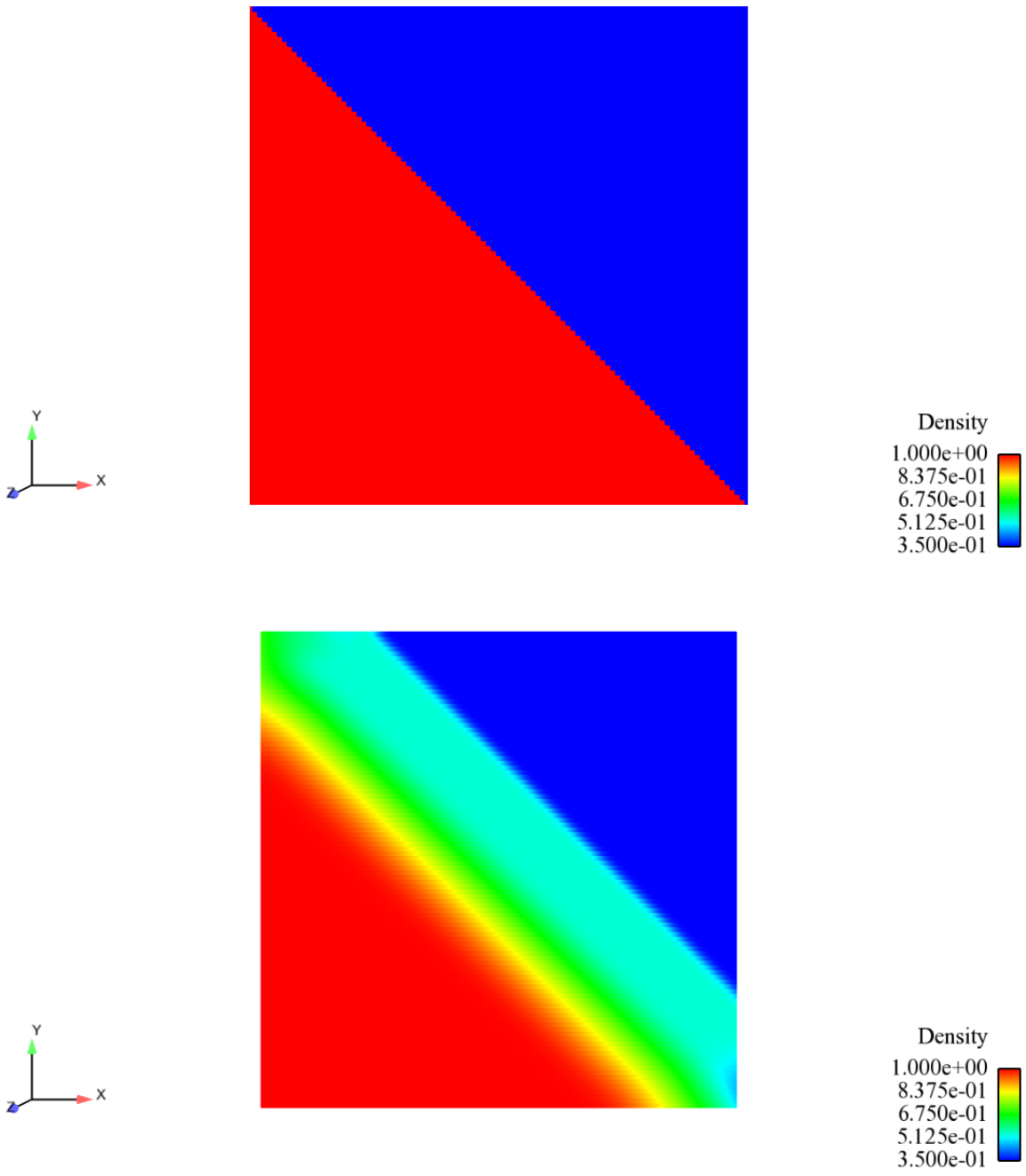

Figure 1: Shock tube with noise: density contours at times $t = 0$ (top) and $t = 4 \times 10^{-4}$ (bottom). The CFL is $1/2$.

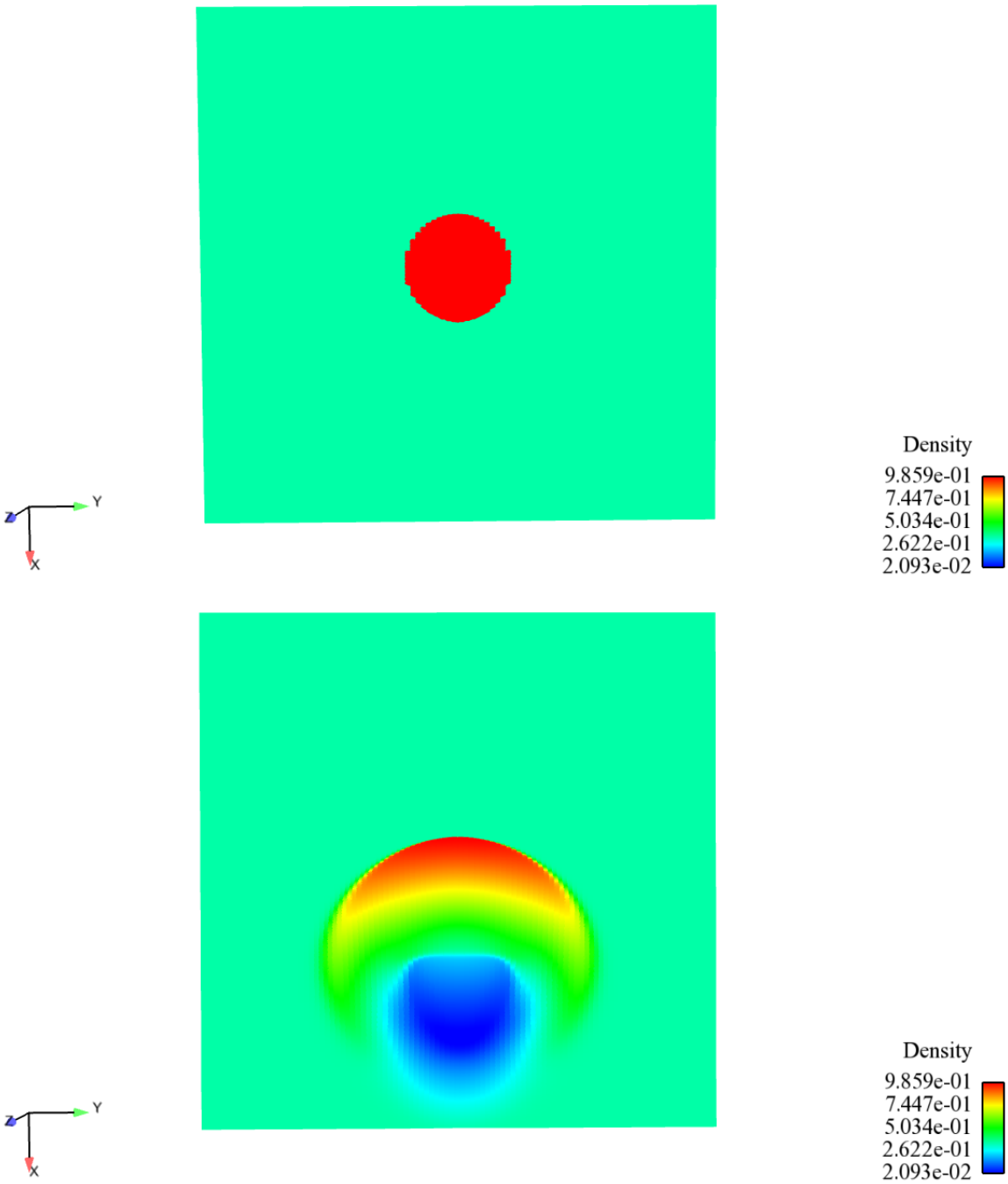

Figure 2: Collapse on a moving surface with noise: density contours at times $t = 0$ (top) and $t = 4 \times 10^{-4}$ (bottom). Coarse mesh including $1000x100$ regular cells. The CFL is $1/2$.

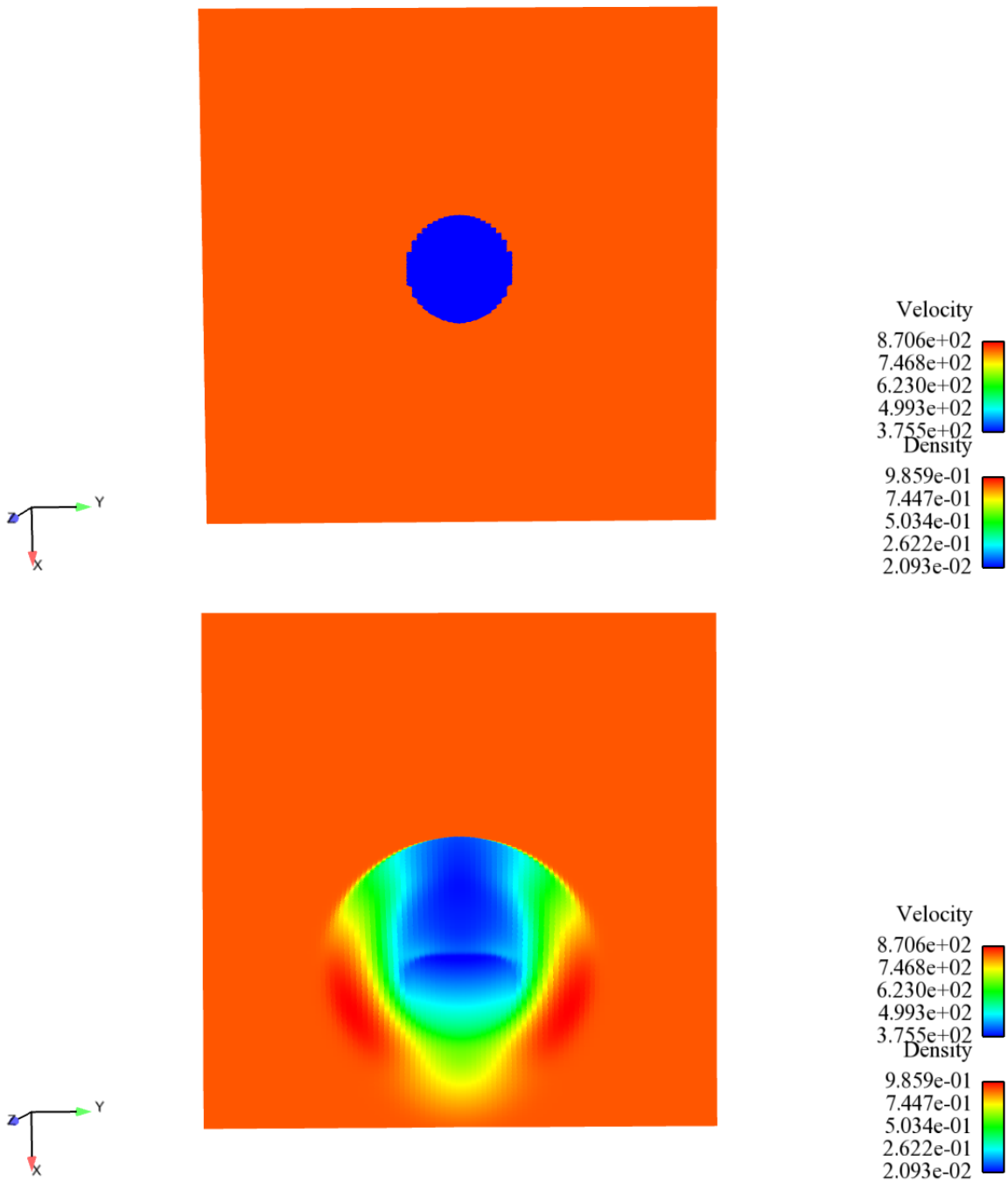

Figure 3: Collapse on a moving surface with noise: velocity contours at times $t = 0$ (top) and $t = 4 \times 10^{-4}$ (bottom). Coarse mesh including $1000x100$ regular cells. The CFL is $1/2$.

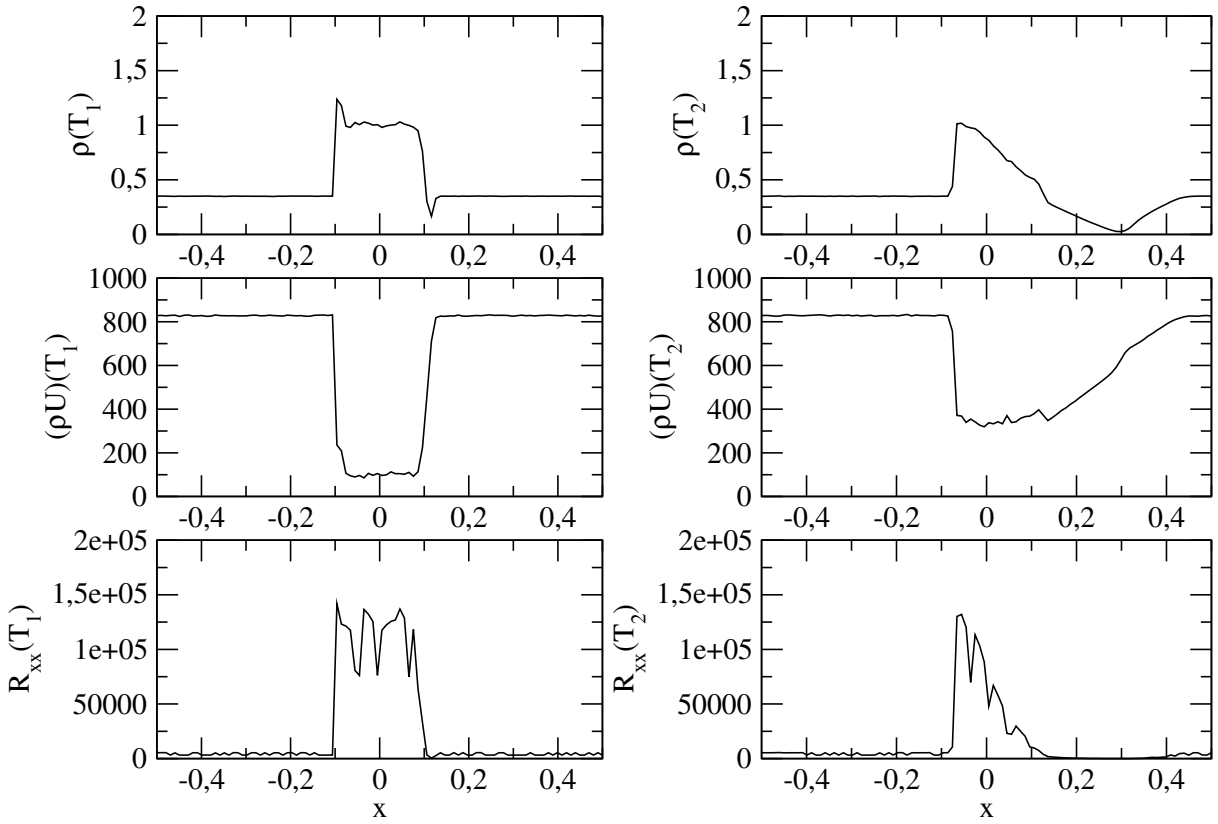

Figure 4: Collapse on a moving surface with noise: density (top) and x-momentum profiles at times $t = T_1 = 5 \times 10^{-5}$ (left) and $t = T_2 = 4 \times 10^{-4}$ (right) along the line $y = 0$, together with R_{xx} component (bottom). Coarse mesh including $1000x100$ regular cells. The CFL is $1/2$.

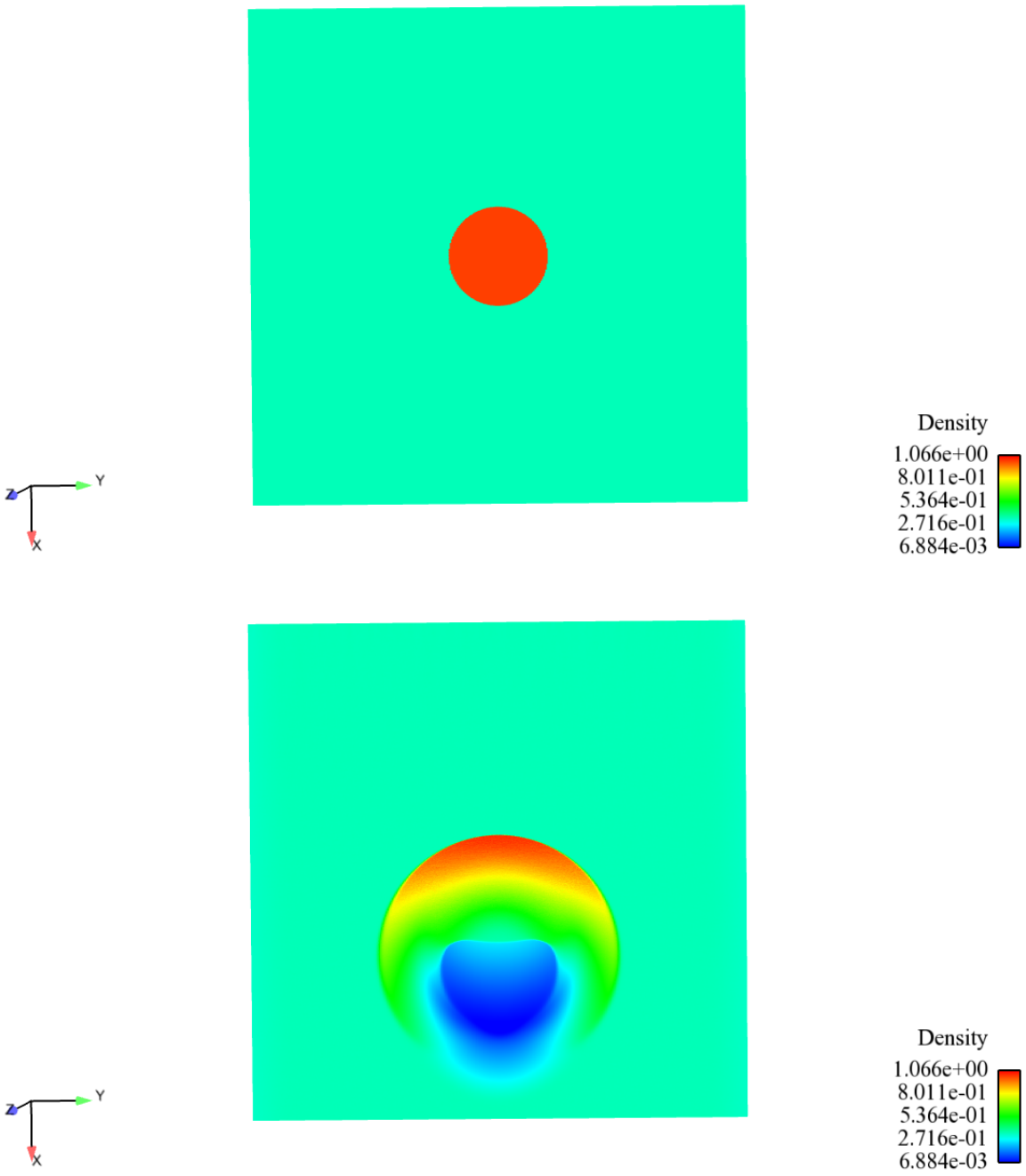

Figure 5: Collapse on a moving surface with noise: density contours at times $t = 0$ (top) and $t = 4 \times 10^{-4}$ (bottom). This fine mesh includes 4000x400 regular cells. The CFL is $1/2$.

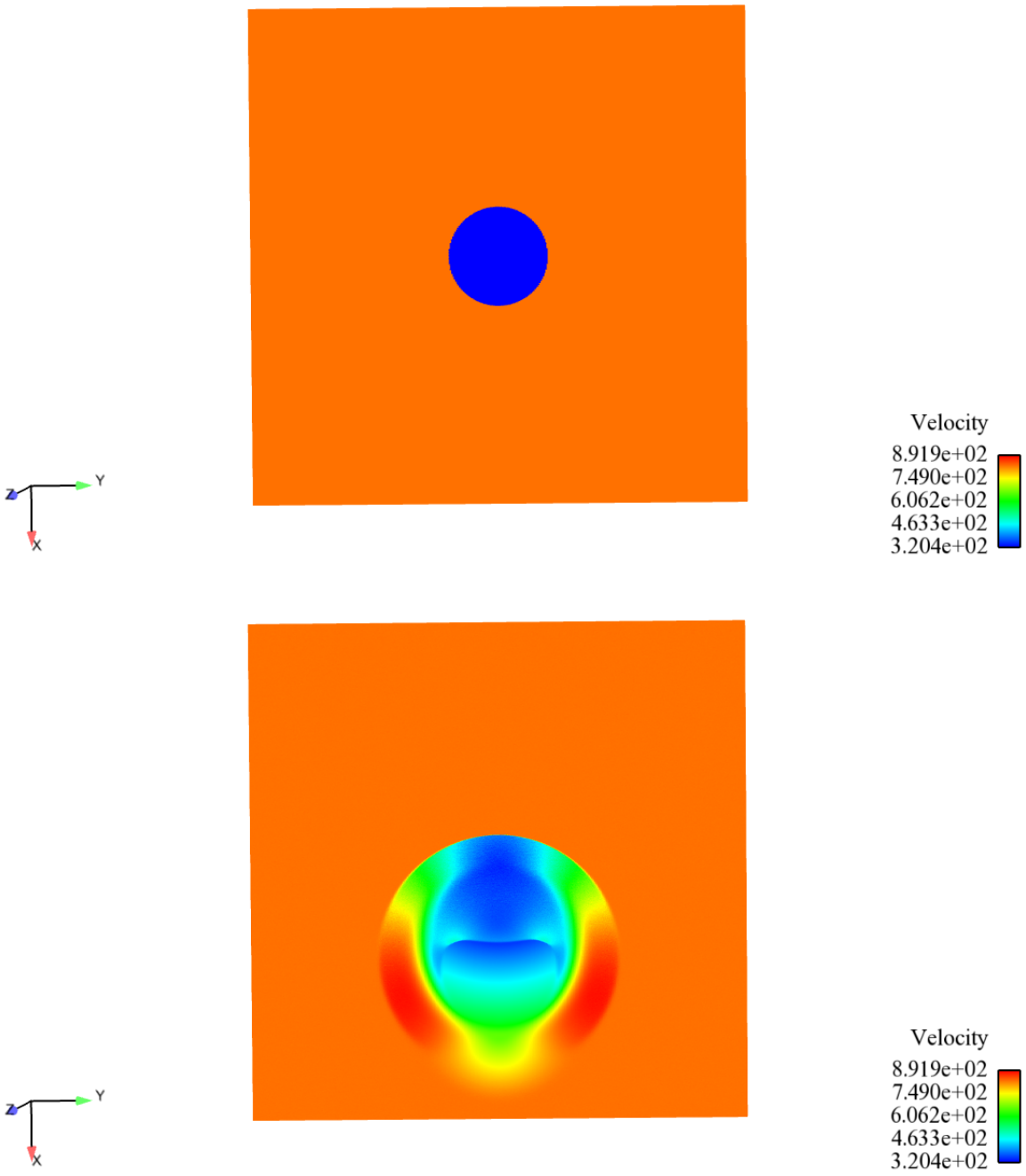

Figure 6: Collapse on a moving surface with noise: velocity contours at times $t = 0$ (top) and $t = 4 \times 10^{-4}$ (bottom). This fine mesh includes $4000x400$ regular cells. The CFL is $1/2$.

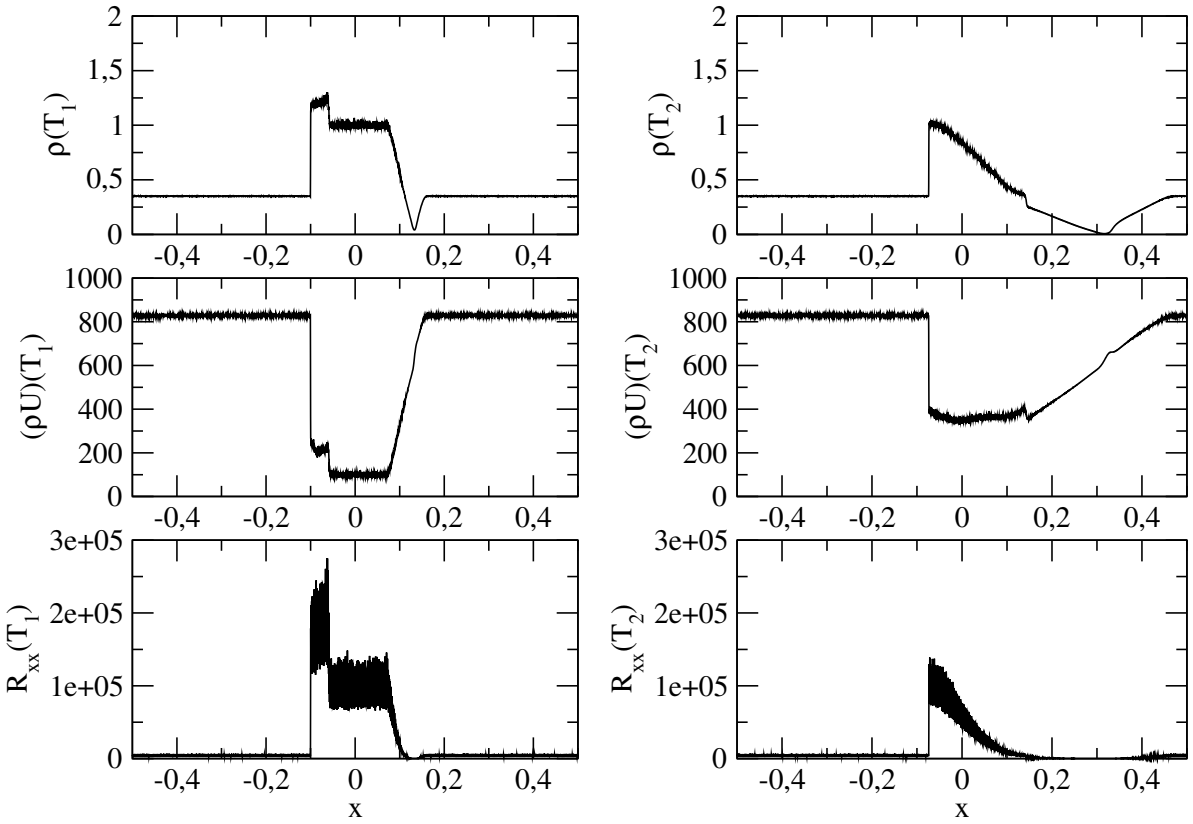

Figure 7: Collapse on a moving surface with noise: density (top) and x-momentum profiles at times $t = T_1 = 5 \times 10^{-5}$ (left) and $t = T_2 = 4 \times 10^{-4}$ (right) along the line $y = 0$, together with R_{xx} component (bottom). This fine mesh includes $4000x400$ regular cells. The CFL is $1/2$.

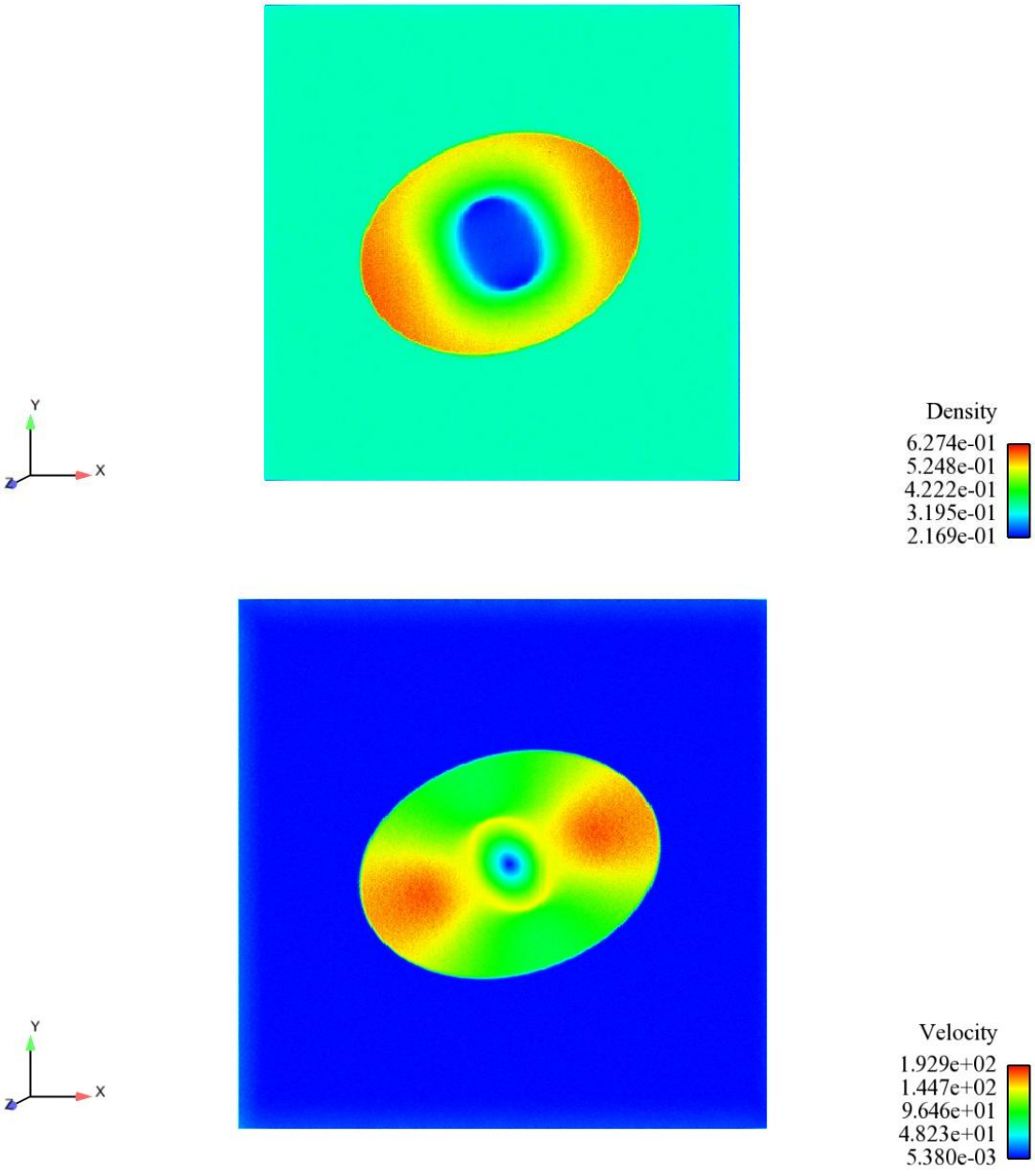

Figure 8: Anisotropic collapse with noise: density (top) and velocity contours (bottom) at time $t = 4 \times 10^{-4}$. Fine mesh including $1000x1000$ regular cells, with $CFL = 1/2$.